

Imaginary Time Propagation on a Quantum Chip

F. Turro,^{1,2,*} V. Amitrano,^{1,2} P. Luchi,^{1,2} K. A. Wendt,³ J. L. Dubois,³ S. Quaglioni,³ and F. Pederiva^{1,2}

¹*Physics Department, University of Trento, Via Sommarive 14, I-38123 Trento, Italy*

²*INFN-TIFPA Trento Institute of Fundamental Physics and Applications, Trento, Italy*

³*Lawrence Livermore National Laboratory, P.O. Box 808, L-414, Livermore, California 94551, USA*

(Dated: March 1, 2025)

Evolution in imaginary time is a prominent technique for finding the ground state of quantum many-body systems, and the heart of a number of numerical methods that have been used with great success in quantum chemistry, condensed matter and nuclear physics. We propose an algorithm to implement imaginary time propagation on a quantum computer. Our algorithm is devised in the context of an efficient encoding into an optimized gate, drawing on the underlying characteristics of the quantum device, of a unitary operation in an extended Hilbert space. However, we proved that for simple problems it can be successfully applied to standard digital quantum machines. This work paves the way for porting quantum many-body methods based on imaginary-time propagation to near-term quantum devices, enabling the future quantum simulation of the ground states of a broad class of microscopic systems.

As originally proposed by Feynman in the 1980's [1], quantum computers are theorized to be exponentially more efficient than any classical algorithm in the description of non-relativistic quantum many-body system. A notoriously hard problem for a classical computer is to find the ground state of a complex many-body system, be it in chemistry, condensed matter or nuclear physics. In most many-body methods, such as configuration-interaction or coupled-cluster, the main limiting factor is the exponential growth of the model space with increasing number of particles or increased fidelity of the calculation. On the other hand, in quantum Monte Carlo methods applied to Fermionic systems one has to contend with an exponential increase of the computing time with the number of particles caused by the emergence of the Fermion sign problem, which has been argued to be a NP-hard problem [2]. There is therefore a desire to develop quantum versions of prominent quantum many-body methods, and in particular quantum algorithms that can be efficiently applied to emerging prototypes of quantum computing platforms, which suffer from limitations in gate error rates and quantum-device noise.

Many classical algorithms for the calculation of the ground state of microscopic systems, including projection Monte Carlo techniques, are based on the Imaginary Time Propagation (ITP) method (for an application in nuclear structure theory see e.g. Ref. [3]). In a nutshell, this consists of solving the time-dependent Schrödinger equation along the imaginary time axis, rather than along the real time one (the so-called Wick rotation). The resulting evolution operator causes the exponential decay of the amplitude of all states with respect to the ground state one. Such operator can then be applied to compute the actual ground state (in mathematical sense) of any given Hamiltonian starting from an arbitrary state that is not orthogonal to the ground state itself. A method

to simulate imaginary time evolution on a quantum computer using a hybrid quantum-classical variational algorithm was proposed in Ref. [4]. Other hybrid quantum-classical approaches for computing ground states include the variational quantum eigensolver [5], which has been applied to several quantum systems [6–13] and the quantum approximate optimisation algorithm proposed in Ref. [14]. In these coprocessing algorithms the classical computer takes care of the optimisation of the parameters of a variational wave function while a *universal* quantum computer is used to perform a relatively small number of discrete qubit operations (gates) within a finite universal set. The use of such shallow quantum circuits is a common strategy to reduce the adverse impact of noise, enabling the application of the algorithm on present-day and near-term quantum hardware.

In this paper we propose a method to implement ITP on a quantum computer by means of a purely quantum algorithm. While the real-time propagator of a quantum mechanical system is a unitary operator, the corresponding imaginary-time propagator is not, and cannot be directly translated into a quantum gate. Therefore, we devise a unitary operator that implements the ITP by working within an extended Hilbert space, given by the tensor product of the computational model space with a reservoir qubit. The approach of realizing a quantum simulation by working in an extended Hilbert space was first proposed in Ref. [15]. We study the accuracy of this method in applications to the Hydrogen atom and a simple nuclear system [16] by comparing an exact, classical simulation with the results obtained by implementing a circuit of primitive gates on a universal quantum computer (namely the freely accessible QPUs of the IBM Quantum Experience system), and by simulating the implementation of optimal quantum control on the superconducting three-dimensional (3D) transmon qudit of Ref. [17]. These are two of the currently available quantum computing platforms.

Before introducing the quantum version of the algorithm, here we briefly recall the basic ITP method (ad-

* francesco.turro@unitn.it

ditional detail can be found, for example, in Ref. [3]).

Given a time-independent Hamiltonian H , an arbitrary state $|\psi\rangle$ belonging to the Hilbert space of H can be evolved in imaginary time $\tau = it$ (with t the real time) by formally applying the propagator $e^{-\hat{H}\tau}$ according to:

$$|\psi(\tau)\rangle = e^{-\hat{H}\tau} |\psi(0)\rangle = \sum_{n=0}^{\infty} c_n e^{-E_n \tau} |\phi_n\rangle, \quad (1)$$

where we have decomposed the initial state at time $t = 0$ ($\tau = 0$) in terms of the eigenvectors $|\phi_n\rangle$ of the Hamiltonian, with eigenvalue E_n . We notice that the imaginary-time propagator is hermitian but not unitary. In general, this causes the normalization of the evolved state and of its components not to be preserved. It is possible to keep constant at least the normalization of the ground state, modifying the propagator in the following way:

$$|\psi(\tau)\rangle = e^{-\tau(\hat{H}-E_T)} |\psi(0)\rangle. \quad (2)$$

If E_T is chosen as the ground state energy E_0 , Eq. (1) shows that, in imaginary time, any arbitrary state non orthogonal to the ground state $|\phi_0\rangle$ evolves to the mathematical ground state of \hat{H} because the components along the excited states are exponentially suppressed. In practical applications it is not necessary to know in advance the exact value of E_0 , but it is sufficient to have a reasonable approximation, such as a variational estimate. In order to reproduce this algorithm on a quantum computer, we need to take into account the intrinsic non-unitarity of the process. One possibility to implement a dissipative process is to extend the Hilbert space coupling it to a reservoir, and transfer probability to the components of the computational basis orthogonal to the original Hilbert space. Let us map an arbitrary state of the physical system onto a (multi)qubit state $|\psi_s\rangle$. We then introduce the product state of $|\psi_s\rangle$ with a reservoir qubit prepared in the $|0\rangle$ state, yielding the total initial wave function:

$$|\Psi_{\text{init}}\rangle = |0\rangle \otimes |\psi_s\rangle = \begin{pmatrix} 1 \\ 0 \end{pmatrix} \otimes |\psi_s\rangle, \quad (3)$$

and the unitary operator acting on the total Hilbert space (system times reservoir qubit)

$$\hat{U}(\tau) = \begin{pmatrix} \hat{Q}_{\text{ITP}}(\tau) & (\mathbb{1} + e^{-2(\hat{H}-E_T)\tau})^{-\frac{1}{2}} \\ (\mathbb{1} + e^{-2(\hat{H}-E_T)\tau})^{-\frac{1}{2}} & -\hat{Q}_{\text{ITP}}(\tau) \end{pmatrix}. \quad (4)$$

Each matrix element in Eq. (4) is an operator acting on the Hilbert space describing the physical system, with

As a demonstration, we applied our quantum ITP

$\hat{Q}_{\text{ITP}}(\tau) = (\mathbb{1} + e^{-2(\hat{H}-E_T)\tau})^{-1/2} e^{-(\hat{H}-E_T)\tau}$ and $\mathbb{1}$ being, respectively, the imaginary-time propagator and the identity operator. (A proof that $U(\tau)$ is a unitary operator is provided in the supplemental material). Notice that $U(\tau)$ can also be written as the sum of the tensor products $\hat{Q}_{\text{ITP}}(\tau) \otimes \hat{\sigma}_z$ and $(\mathbb{1} + e^{-2(\hat{H}-E_T)\tau})^{-1/2} \otimes \hat{\sigma}_x$, where $\hat{\sigma}_z$ and $\hat{\sigma}_x$ are the Pauli Z and X operators acting on the reservoir qubit. The application of $\hat{U}(\tau)$ to $|\Psi\rangle$ yields:

$$|\Psi(\tau)\rangle = |0\rangle \otimes \hat{Q}_{\text{ITP}}(\tau) |\psi_s\rangle + |1\rangle \otimes (\mathbb{1} + e^{-2(\hat{H}-E_T)\tau})^{-\frac{1}{2}} |\psi_s\rangle. \quad (5)$$

It follows that, performing a measurement along the reservoir state $|0\rangle$, the total system collapses to the state:

$$|\Psi_{\text{fin}}\rangle = C |0\rangle \otimes \hat{Q}_{\text{ITP}}(\tau) |\psi_s\rangle, \quad (6)$$

where C is a coefficient introduced to normalize the state after the measurement. Aside from the presence of an additional operator related to the normalization, Eq. (6) corresponds to the standard imaginary time propagator applied to the initial wave function of Eq. (2). More generally, one can prove that $|\psi_s(\tau)\rangle = \hat{Q}_{\text{ITP}}(\tau) |\psi_s\rangle$ is closer to the ground state of \hat{H} than the initial state. In fact, the overall effect of $\hat{Q}_{\text{ITP}}(\tau)$ can be computed in two important limits:

- The limit for $\tau \rightarrow 0$. In this limit, expanding at first order in τ , one can show that:

$$(\mathbb{1} + e^{-2(\hat{H}-E_T)\tau})^{-1/2} \simeq \frac{1}{\sqrt{2}} e^{(\hat{H}-E_T)\tau/2},$$

and hence the action of $\hat{Q}_{\text{ITP}}(\tau)$ corresponds to the application of a classical ITP algorithm, but over an imaginary-time interval $\frac{\tau}{2}$. This limit is useful when adopting a Trotter-Suzuki decomposition of the Hamiltonian.

- The limit for $\tau \gg 1$ (in particular when $\tau \gg \frac{1}{E_1 - E_0}$ where E_1 is the energy of the first excited state and E_0 is the ground state energy. In this limit, the ground state $|\phi_0\rangle$ of the system can be obtained with a single application of the operator \hat{Q}_{ITP} . Indeed, since according to the ITP method one has $e^{-(\hat{H}-E_T)\tau} |\psi_s\rangle \rightarrow c_0 |\phi_0\rangle$ where $c_0 = \langle \phi_0 | \psi_s \rangle$, it follows that $\hat{Q}_{\text{ITP}}(\tau) |\psi_s\rangle \rightarrow \frac{c_0}{\sqrt{2}} |\phi_0\rangle$.

One can also observe that, after the measurements, the final state of the system and reservoir qubits are in the same initial condition as in Eq. (3). Therefore, repeating this algorithm N times yields the evolution for a total imaginary time $\tau_{\text{tot}} > N \frac{\tau}{2}$. algorithm to two physical problems: finding the ground

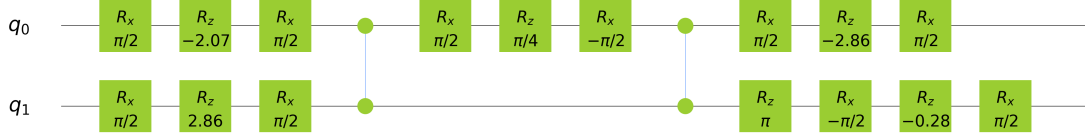


FIG. 1: Gate set for implementing $U(\tau)$ for the Hydrogen atom Hamiltonian with $\tau = 60$ Hartee $^{-1}$. q_0 represents the reservoir qubit and q_1 the system qubit.

state of the Hydrogen atom, and the search of the lowest energy spin state of two neutrons at a given distance, as described in Ref. [16]. For the Hydrogen atom, we implemented in turn two different strategies, i.e. express the unitary transformation in terms of standard quantum gates (namely, R_x , R_z and cZ), and the optimal control approach for a transmon qudit as discussed in Ref. [16]. For the two neutron system, we opted for the optimal control method only. More details are reported in the supplemental material. Experimentally, the occupation probability of each state in the computational basis when the system has reached the ground state, $p_\beta(\tau_{\text{tot}}) = |\langle \beta | \psi_s(\tau_{\text{tot}}) \rangle|^2$, can be obtained starting from the occupancies measured when the reservoir qubit is in turn measured in the $|0\rangle$ state, $p_{0\beta}$, according to the following expression:

$$p_\beta(\tau_{\text{tot}}) = \frac{p_{0\beta}(\tau_{\text{tot}})}{\sum_{i \in \{\beta\}} p_{0i}(\tau_{\text{tot}})}. \quad (7)$$

where β indicates the index of physical state (for n qubit β runs from 0 to $2^n - 1$).

In the simulation of the Hydrogen atom, we assume spherical symmetry and expand the radial wave function on the STO-2G basis, i.e. a linear combination of two Gaussian functions that approximate a Slater-type orbital [18]. Because this is a non-orthogonal basis, before applying our quantum algorithm, we first orthonormalize the Hamiltonian matrix by following the methodology for the solution of a generalized eigenvalue problem (see, e.g., Eq. (5.15) of Ref. [19]). The quantum ITP algorithm requires two qubits: one qubit to represent the two orthonormalized basis states plus an additional reservoir qubit.

We prepare the system-plus-reservoir wave function in the initial condition of Eq. (3) in the spin triplet state, and apply our quantum ITP algorithm in a ‘single shot’ (i.e., working in the $\tau \gg 1$ limit) using $\tau_{\text{tot}} = \tau = 60.0$ Hartee $^{-1}$.

The gate set and the quantum circuit needed to implement the $U(\tau = 60 \text{ Hartee}^{-1})$ operator for the Hydrogen atom Hamiltonian expanded using the STO-2G basis set is shown in Fig. 1.

This quantum circuit has been run on the free access IBM *ibmq_ourense* system [20] with 8192 shots. Results In this example, the extended Hilbert space is covered

are compared to a device level simulation of the implementation on a generic multilevel transmon, similarly to what is described in Ref. [16], with the optimal control approach.

Table I shows the simulated occupation probabilities $p_{\alpha\beta}(\tau_{\text{tot}}) = |\langle \alpha\beta | \Psi(\tau_{\text{tot}}) \rangle|^2$ of the four computational states forming the extended Hilbert space after the application of $U(\tau)$. The final result upon normalization is also shown in Fig. 2. One can see that the final state is essentially the ground state for the optimal control simulation and quite close to it in the IBM results. The difference between IBM and exact values is due to noise and to the internal IBM compilation between the theoretical circuit and the actual gates.

TABLE I: Occupation probabilities for the extended $[P_{\alpha\beta}(\tau_{\text{tot}})]$ and Hydrogen atom $[p_\beta(\tau_{\text{tot}})]$ wave function at the end of the quantum ITP simulation with $\tau = 60.0$ Hartee $^{-1}$ as a function of the computational (2-qubit) basis states $|\alpha\beta\rangle$ for IBM results (IBM) and optimal control simulation (OC). The first digit represents the reservoir state, while the second corresponds to the physical basis state. Also shown are the exact (Exact) occupation probabilities for the ground state. (See the text for additional details.)

$ \alpha\beta\rangle$	$P_{\alpha\beta}^{\text{IBM}}(\tau_{\text{tot}})$	$p_\beta^{\text{IBM}}(\tau_{\text{tot}})$	$P_{\alpha\beta}^{\text{OC}}(\tau_{\text{tot}})$	$p_\beta^{\text{OC}}(\tau_{\text{tot}})$	Exact
$ 00\rangle$	0.033	0.125	0.004	0.024	0.020
$ 01\rangle$	0.236	0.875	0.176	0.976	0.980
$ 10\rangle$	0.417		0.535		
$ 11\rangle$	0.312		0.285		

As a second example, we apply our quantum ITP algorithm to a system of two neutrons interacting with a chiral effective field theory (χ -EFT) nucleon-nucleon potential at leading order (LO) [21, 22]. A detailed expression for the Hamiltonian is given in the supplemental material, but we should mention here that it is characterized by a spin-state dependence that includes full tensorial terms. As previously done in Ref. [16], we consider the simplified case in which the two neutrons are ‘frozen’ in space, reducing the problem to the description of two spins interacting through the nuclear Hamiltonian at fixed separation.

by the first 8 levels (3 qubits) of a qudit, representing

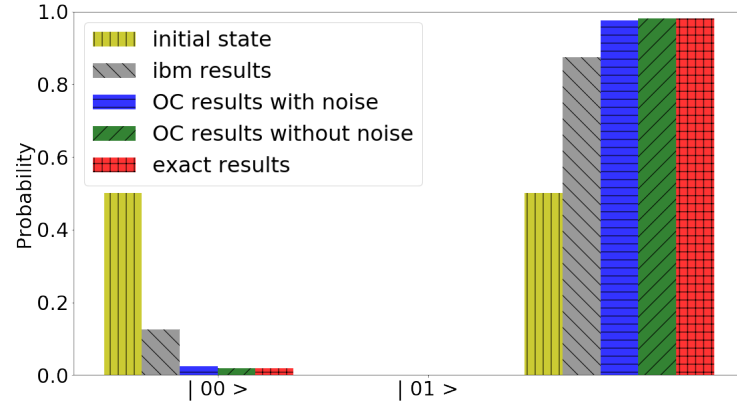


FIG. 2: Normalized occupation probabilities (p_β) for the computed wave function of the Hydrogen atom using the STO-2G basis set at $\tau = 0$ (yellow bar) and $\tau = 60.0 \text{ Hartee}^{-1}$ in two different approaches: the IBM result (grey bar) and the optimal control with (blue bar) and without (green bar) inclusion of hardware noise compared to the exact ground-state distribution (red bar).

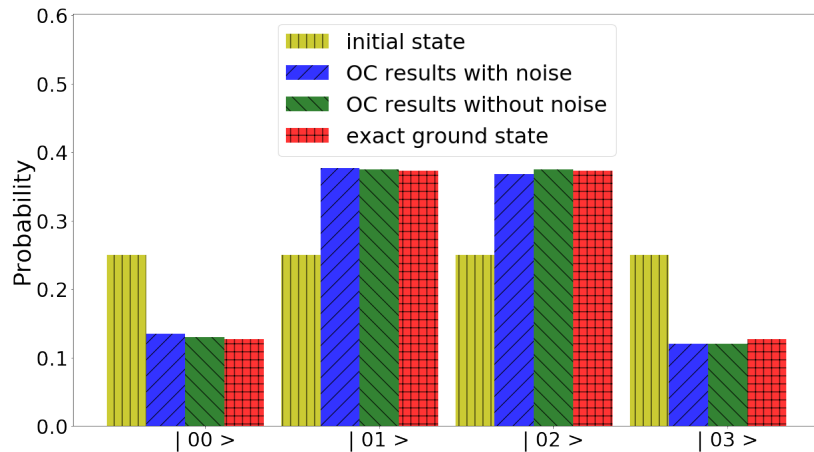


FIG. 3: Normalized occupation probabilities (p_β) for the computed wave function of the two-neutron system at $\tau = 0$ (yellow bar) and $\tau = 1 \text{ MeV}^{-1}$ with (blue bar) and without (green bar) inclusion of hardware noise compared to the exact ground-state distribution (red bar). (See the text for additional information.)

the tensor product between the 4 levels (2 qubits) used to describe the spin state of the two neutrons, and the two levels of the reservoir qubit. The mapping of the computational states to the quantum processor is as follows: the $|0\rangle$ Fock state corresponds to the tensor product of the reservoir qubit in state $|0\rangle$ with the uncoupled spin state of $|0\rangle \otimes |\downarrow\downarrow\rangle$. Likewise, $|1\rangle$, $|2\rangle$, and $|3\rangle$ correspond, respectively, to the tensor products with the uncoupled spin states $|0\rangle \otimes |\downarrow\uparrow\rangle$, $|0\rangle \otimes |\uparrow\downarrow\rangle$, and $|0\rangle \otimes |\uparrow\uparrow\rangle$. The next four Fock states have a similar mapping, except for the reservoir qubit being in the $|1\rangle$ state.

The system is initially prepared in the state $|\psi_s(\tau = 0)\rangle = \frac{1}{2}(|0\rangle + |1\rangle + |2\rangle + |3\rangle)$. As before, we work in the limit $\tau \gg 1$, in particular, we simulated a single propagation over an imaginary time $\tau_{\text{tot}} = \tau = 1 \text{ MeV}^{-1}$. In Fig. 3 we present the simulated occupation probabilities of the two neutrons spin states. Once

again, the probability distribution is already very close to that of the exact ground state.

The robustness of the algorithm is discussed in the supplemental material, where we also show how the final state depends on the choice of the parameter E_T in the propagator.

In this letter, we proposed a quantum version of the Imaginary Time Propagation algorithm for an arbitrary Hamiltonian. The method was tested and validated for two different, simple physical problems: find the ground state of the Hydrogen atom expanded over a STO-2G basis set, and the spin ground state of two neutrons interacting with a realistic nuclear Hamiltonian and kept at fixed distance. We showed that a single application of the propagator over a sufficiently large imaginary time interval is enough to obtain a very good approximation of the ground state. Moreover, we have tested both at

device level simulation and on a real quantum computer the robustness of the algorithm against quantum noise, proving its potential for solving more general problems in fields like nuclear structure, solid state physics or quantum chemistry.

As in the classical ITP algorithms, one of the main problems is the choice of the initial state. In particular, starting from a state loosely overlapped to the ground state implies the need of a very large number of repetitions of the measurements in order to reach

a reasonable accuracy, since the normalization of the ground state is halved at each application of the propagator. This can be solved either by coupling the method with effective methods for preparing the initial state [23].

FT is supported by the Q@TN grant ANuPC-QS. PL is supported by the Q@TN grant ML-QForge. This work was prepared in part by LLNL under Contract DE-AC52-07NA27344 with support from the Laboratory Directed Research and Development grant 19-DR-005.

[1] R. P. Feynman, International Journal of Theoretical-Physics21, 467 (1982).

[2] M. Troyer and U.-J. Wiese, Phys. Rev. Lett.94, 170201(2005).

[3] F. Pederiva, A. Roggero, and K. E. Schmidt, An Advanced Course in Computational Nuclear Physics: Bridging theScales from Quarks to Neutron Stars (Springer International Publishing, 2017) pp. 401–476.

[4] S. McArdle, T. Jones, Y. Endo, Suguru and Li, S. C.Benjamin, and X. Yuan, npj Quantum Information5,75 (2019).

[5] A. Peruzzo, J. McClean, P. Shadbolt, M. H. Yung, X. Q.Zhou, P. J. Love, A. Aspuru-Guzik, and J. L. O'Brien,Nature Communications5, 4213 (2014).

[6] Y. Wang, F. Dolde, J. Biamonte, R. Babbush,V. Bergholm, S. Yang, I. Jakobi, P. Neumann,A. Aspuru-Guzik, J. D. Whitfield, and J. Wrachtrup,ACS Nano9, 7769 (2015)

[7] P. J. J. O'Malley, R. Babbush, I. D. Kivlichan,J. Romero, J. R. McClean, R. Barends, J. Kelly, P. Roushan, A. Tranter, N. Ding, B. Campbell, Y. Chen,Z. Chen, B. Chiaro, A. Dunsworth, A. G. Fowler, E. Jeffrey, E. Lucero, A. Megrant, J. Y. Mutus, M. Neeley,C. Neill, C. Quintana, D. Sank, A. Vainsencher, J. Wenner, T. C. White, P. V. Coveney, P. J. Love, H. Neven,A. Aspuru-Guzik, and J. M. Martinis, Phys. Rev. X6,031007 (2016)

[8] P. Roushan, A. Tranter, N. Ding, B. Campbell, Y. Chen,Z. Chen, B. Chiaro, A. Dunsworth, A. G. Fowler, E. Jeffrey, E. Lucero, A. Megrant, J. Y. Mutus, M. Neeley,C. Neill, C. Quintana, D. Sank, A. Vainsencher, J. Wenner, T. C. White, P. V. Coveney, P. J. Love, H. Neven,A. Aspuru-Guzik, and J. M. Martinis, Phys. Rev. X6,031007 (2016)

[9] J. R. McClean, J. Romero, R. Babbush, and A. Aspuru-Guzik, New Journal of Physics18, 023023 (2016)

[10] S. Paesani, A. A. Gentile, R. Santagati, J. Wang,N. Wiebe, D. P. Tew, J. L. O'Brien, and M. G. Thompson, Phys. Rev. Lett.118, 100503 (2017)

[11] J. I. Colless, V. V. Ramasesh, D. Dahmen, M. S. Blok,M. E. Kimchi-Schwartz, J. R. McClean, J. Carter, W. A.de Jong, and I. Siddiqi, Phys. Rev. X8, 011021 (2018)

[12] E. F. Dumitrescu, A. J. McCaskey, G. Hagen, G. R.Jansen, T. D. Morris, T. Papenbrock, R. C. Pooser, D. J.Dean, and P. Lougovski, Phys. Rev. Lett.120, 210501(2018)

[13] H. Lu, N. Klco, J. M. Lukens, T. D. Morris, A. Bansal, A. Ekström, G. Hagen, T. Papenbrock, A. M. Weiner,M. J. Savage, and P. Lougovski, Phys. Rev. A100,012320 (2019)

[14] E. Farhi, J. Goldstone, and S. Gutmann

[15] Z. B. Walters, (2015), [arXiv:1510.00409](https://arxiv.org/abs/1510.00409) [physics.gen-ph]

[16] E. T. Holland, K. A. Wendt, K. Kravvaris, X. Wu, W. E.Ormand, J. L. DuBois, S. Quaglioni, and F. Pederiva,Phys. Rev. A101, 062307 (2020)

[17] X. Wu, S. L. Tomarken, N. A. Petersson, L. A. Martinez,Y. J. Rosen, and J. L. DuBois, Phys. Rev. Lett.125,170502 (2020)

[18] W. J. Hehre, R. F. Stewart, and J. A. Pople, The Journal of Chemical Physics51, 2657 (1969)

[19] P. Löwdin, The Journal of Chemical Physics18, 365(1950)

[20] <https://quantum-computing.ibm.com/>

[21] A. Gezerlis, I. Tews, E. Epelbaum, M. Freunek, S. Gandolfi, K. Hebeler, A. Nogga, and A. Schwenk, Phys. Rev.C90, 054323 (2014)

[22] I. Tews, S. Gandolfi, A. Gezerlis, and A. Schwenk, Phys. Rev. C93, 024305 (2016)

[23] A. Roggero, C. Gu, A. Baroni, and T. Papenbrock, Phys. Rev. C102, 064624 (2020).

[24] N. Khaneja and T. Reiss and C. Kehlet and T. Schulte-Herbrüggen and S. J. Glaser, J. Magn. Reson. 172, 296 (2005)

[25] J. Johansson, P. Nation, and F. Nori, Computer Physics Communications 184, 1234 (2013)

Supplemental Material

S1. UNITARITY OF THE ITP PROPAGATOR

$$U(\tau) = \hat{\sigma}_x \otimes \frac{1}{\sqrt{1 + e^{-2(\hat{H}-E_T)\tau}}} + \hat{\sigma}_z \otimes \hat{Q}_{\text{ITP}}(\tau). \quad (\text{S8})$$

The operator $U(\tau)$ in Eq. (4) of the main text can also be written as:

Here we show in eq. (S9) that the operator $U(\tau)$ is unitary.

$$\begin{aligned} U^\dagger U &= \begin{pmatrix} e^{-(\hat{H}-E_T)\tau} & \mathbb{1} \\ \mathbb{1} & -e^{-(\hat{H}-E_T)\tau} \end{pmatrix} \frac{1}{\sqrt{1 + e^{-2(\hat{H}-E_T)\tau}}} \frac{\mathbb{1}}{\sqrt{1 + e^{-2(\hat{H}-E_T)\tau}}} \begin{pmatrix} e^{-(\hat{H}-E_T)\tau} & \mathbb{1} \\ \mathbb{1} & -e^{-(\hat{H}-E_T)\tau} \end{pmatrix} \\ &= \frac{\mathbb{1}}{1 + e^{-2(\hat{H}-E_T)\tau}} \begin{pmatrix} e^{-(\hat{H}-E_T)\tau} & \mathbb{1} \\ \mathbb{1} & -e^{-(\hat{H}-E_T)\tau} \end{pmatrix} \begin{pmatrix} e^{-(\hat{H}-E_T)\tau} & \mathbb{1} \\ \mathbb{1} & -e^{-(\hat{H}-E_T)\tau} \end{pmatrix} \\ &= \frac{\mathbb{1}}{1 + e^{-2(\hat{H}-E_T)\tau}} \begin{pmatrix} \mathbb{1} + e^{-2(\hat{H}-E_T)\tau} & 0 \\ 0 & 1 + e^{-2(\hat{H}-E_T)\tau} \end{pmatrix} = \begin{pmatrix} \mathbb{1} & 0 \\ 0 & \mathbb{1} \end{pmatrix} \end{aligned} \quad (\text{S9})$$

In the proof we used the fact that the operators $\mathbb{1}$ and $e^{-(\hat{H}-E_T)\tau}$ are self-adjoint. Also, in the second line of eq. (S9), we have used that the factor $\frac{1}{1 + e^{-2(\hat{H}-E_T)\tau}}$ commutes with the identity and $e^{-(\hat{H}-E_T)\tau}$.

S2. OPTIMAL CONTROL APPROACH

To implement the device level simulations presented in the main text, we mapped the physical system under investigation onto the levels of a superconducting a three-dimensional transmon architecture [16], and solved for the control Hamiltonian $\hat{H}_c(t)$ in the general optimization problem:

$$U(\tau) = \mathcal{T} \exp \left\{ -\frac{i}{\hbar} \int_0^T \left[\hat{H}_d^{(4)} + \hat{H}_c(t) \right] dt \right\}, \quad (\text{S10})$$

where $\hat{H}_d^{(4)}$ is the Hamiltonian for a 3D transmon coupled to a readout cavity (up to forth order in the phase across the Josephson junction), the notation $\mathcal{T} \exp$ stands for a time-ordered exponential, and T is the duration of the control pulse (for additional details, we refer the interested reader to Ref. [16]). Eq. (S10) was solved by means of the Gradient Ascent Pulse Engineering (GRAPE) algorithm [24].

The output of the quantum device is obtained in the presence of realistic quantum hardware noise using the open source quantum optics toolbox (QUTIP) [25]. The unitary operator $U(\tau)$ of Eq. (4) is a $2N$ -by- $2N$ matrix (where N is the total number of physical states),

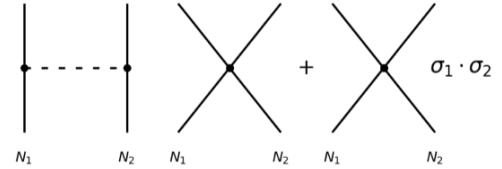


FIG. S4: Schematic description of the leading order nucleon-nucleon interaction. The left diagram depicts a single pion exchange while the middle and right diagrams depict a spin-independent and spin-dependent contact term, respectively.

which we compute using the QUTIP *expm* function. The control pulse is obtained with a 99.9999% fidelity using the same pulse duration ($T = 50$ ns) and maximum drive strength (20 MHz) adopted in Ref. [16]. The relaxation time was chosen as $T_1 = 50$ ns and the dephasing time as $T_2 = 7$ ns. The GRAPE code was fed with a pulse initialized using the "ZERO" class of *qutip.control.pulseoptim* (the initial pulse is a complex array of zeros), and the error fidelity threshold was set to less than 10^{-6} .

S3. NUCLEAR HAMILTONIAN

The simplest realistic model of the nucleon-nucleon interaction can be based on the leading order (LO) of a chiral effective field theory (χ -EFT). In this approximation, the nucleon-nucleon interaction is given by the sum of three terms (see Fig. S4). The first describes a mid range interaction due to the exchange of a pion. The second and the third are effective contact terms to be introduced in the renormalization procedure. These terms give rise to spin-independent (SI) and spin-dependent (SD) components, so that the Hamiltonian can be expressed as $H = T + V^{\text{SI}} + V^{\text{SD}}$, where T is the kinetic energy of the nucleons. In this work we are not interested in reproducing the whole dynamics of the particles, but rather in studying the spin dynamics of two neutrons kept at fixed separation. More explicitly, considering a system of two neutrons, we neglect the spin independent terms in H and restrict ourselves to the SD interaction evaluated at a given separation $\vec{r} = \vec{r}_2 - \vec{r}_1$. V^{SD} can then be divided into a vector and a tensor component as

$$V^{\text{SD}} = A_1(\vec{r}) \sum_{\alpha} \sigma_{\alpha}^1 \sigma_{\alpha}^2 + \sum_{\alpha\beta} \sigma_{\alpha}^1 A_2^{\alpha\beta}(\vec{r}) \sigma_{\beta}^2, \quad (\text{S11})$$

where σ are the Pauli matrices acting on the nucleon spin states. $A^1(\vec{r})$ and $A^2(\vec{r})$ can be obtained evaluating the coordinate-dependent parts of the nucleon-nucleon interaction considered (for the explicit functional forms see e.g. Refs. [21, 22]).

S4. ROBUSTNESS OF THE ALGORITHM AGAINST THE CHOICE OF THE TRIAL ENERGY

We studied the energy profiles as function of the trial energy for the Hydrogen atom. We remind that trial energy is the constant in the imaginary time propagator that should guarantee the stability of the normalization of the component along the ground state of the system. The optimal choice is $E_T = E_0$, but in general one has to rely on some approximation to E_0 . A wrong choice might in principle lead to completely unstable results. Fig. S5 (Fig. S6) shows the energy after the propagation as a

function of the trial energy E_T for an imaginary time step $\tau = 5, 10, 20$ Hartree $^{-1}$ in the case $E_T > E_0$ ($E_T < E_0$). One can see that in all cases the propagation yields a state that is a better approximation of the ground state. When $E_T > \sim E_0$ (Fig. S5) the energy corresponding to the projected state is quite close to the expected one. On the contrary, some errors appear in the simulated data when $E_T < E_0$ (Fig. S6). Setting $E_T = E_0 - \Delta$ with $\Delta > 0$ one has that $e^{\tau(H-E_T)} = e^{-\tau(\hat{H}-E_0)} e^{-\tau\Delta}$. In this case, the not-exact ITP propagator for $\tau \gg 1$ rapidly tends to a zero matrix due to the Δ contribution. This causes the effect of driving to ground state of ITP operator $\hat{Q}_{\text{IPT}}(\tau)$ to be negligible. Hence, the final unitary gate $U(\tau)$ eventually reduces to an X gate on the ancilla qubit, implying that the final probability of measuring the ancilla in the $|0\rangle$ state tends to 0. Moreover, in a realistic simulations, the measured probability of the $|0\rangle$ state of the ancilla would exclusively be the result of quantum noise of machine.

S5. DISCUSSION OF THE RESULTS OBTAINED ON THE IBM SYSTEM

We tested the validity of method presented in this paper running the code in Fig. 1 of the main text on different free access IBM Quantum Experience machines [20]. In particular we tested the following QPUs: *ibmq_16_melbourneQPU*, *ibmq_ourense*, *ibmqx2*, *ibmq_essex* and the IBM QPU simulator (*ibmq_qasm_simulator*). All tests were performed using 8192 shots starting from the $\frac{1}{\sqrt{2}}(|0\rangle + |1\rangle)$ state.

The numerical results are shown in Tab. S2 with the theoretical results of the application of $U(\tau)$. Normalized probabilities are plotted in Fig. S7.

There are evidently different degrees of approximation to the exact solution in the results from different machines. The discrepancies can be attributed to errors of IBM compiler that approximates the gates in Fig. 1 on the elementary gates of different QPU and the noise of different machines. The contribution of the noise is more visible in the probability for the $|00\rangle$ state (see Tab. S2) where the values are systematically larger than the expected ones, probably because of the relaxation processes, such as the decay from the excited level to ground state level, occurring in the QPU.

TABLE S2: Result for the occupation probabilities for the extended $[p_{\alpha\beta}(\tau_{\text{tot}})]$ wave function at the end of the quantum ITP simulation with $\tau = 60.0$ Hartee $^{-1}$ as a function of the computational (2-qubit) basis states $|\alpha\beta\rangle$ of different QPU IBM. The index 1 indicates the *ibmq_16_melbourneQPU*, 2 *ibmq_ourense*, 3 *ibmqx2*, 4 *ibmq_essex* and 5 the IBM simulator of QPU. The first digit represents the reservoir state, while the second corresponds to the physical system state. Also shown are the exact (Exact) occupation probabilities.

$ \alpha\beta\rangle$	$p_{\alpha\beta}^1(\tau_{\text{tot}})$	$p_{\alpha\beta}^2(\tau_{\text{tot}})$	$p_{\alpha\beta}^3(\tau_{\text{tot}})$	$p_{\alpha\beta}^4(\tau_{\text{tot}})$	$p_{\alpha\beta}^5(\tau_{\text{tot}})$	Exact
$ 00\rangle$	0.05896	0.02844	0.04224	0.05957	0.00330	0.00357
$ 01\rangle$	0.52063	0.42676	0.54370	0.47827	0.537965	0.53561
$ 10\rangle$	0.18091	0.22766	0.17932	0.18921	0.17688	0.17678
$ 11\rangle$	0.23950	0.31714	0.23474	0.27295	0.28186	0.28403

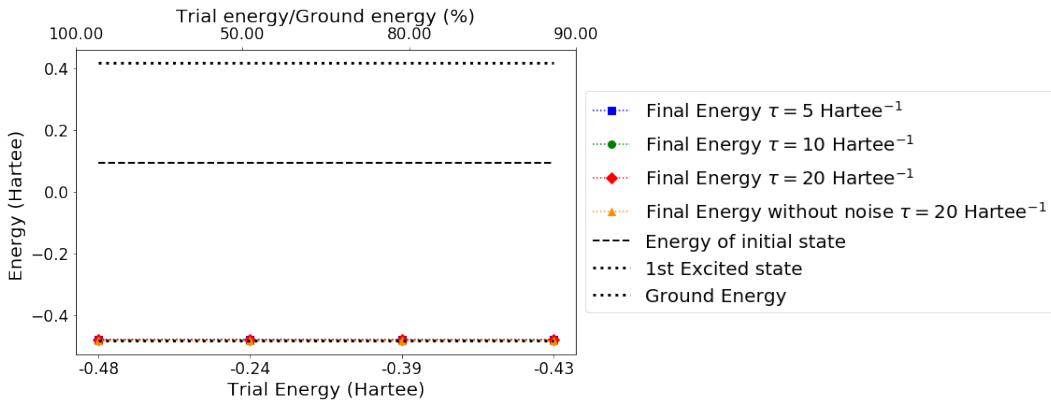


FIG. S5: Plot of the estimated ground-state energy of the Hydrogen atom vs. the trial energies E_T for $\tau = 5, 10, 20$ Hartee $^{-1}$. The first point corresponds to $E_T = E_0$ Hartee. The other points are E_T of 50,80,90 % of E_0 .

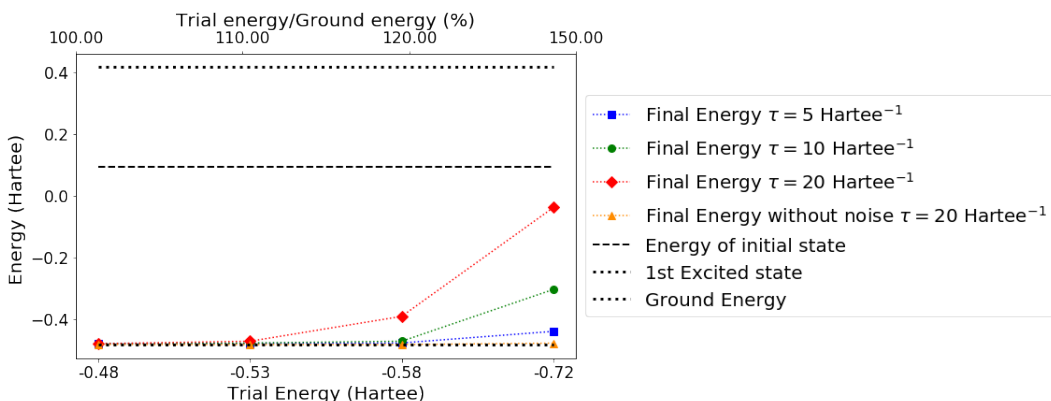


FIG. S6: Plot of the estimated ground-state energy of the Hydrogen atom vs. the trial energies E_T for $\tau = 5, 10, 20$ Hartee $^{-1}$. The first point corresponds to $E_T = E_0$ Hartee. The other points are E_T of 110,120,150% of E_0 .

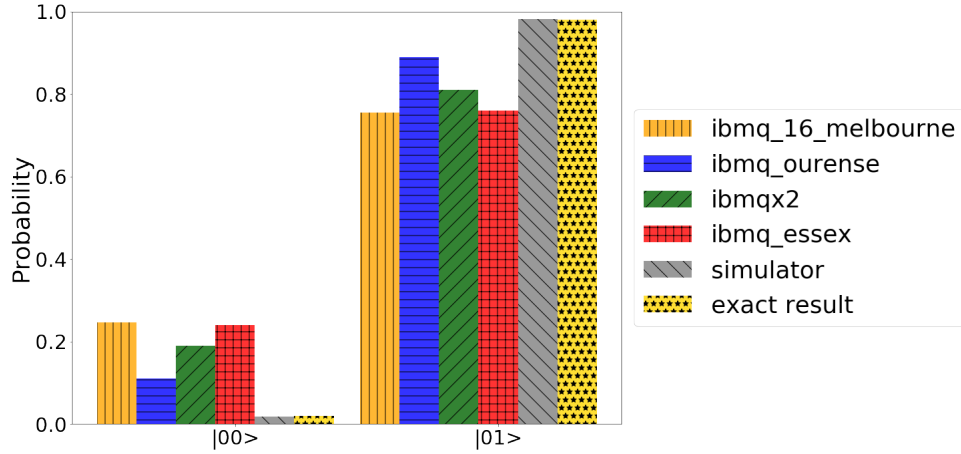


FIG. S7: Normalized occupation probabilities (p_β) for the computed wave function of the Hydrogen atom using the STO-2G basis set at $\tau = 0$ (yellow bar) and $\tau = 60.0$ Hartee $^{-1}$ in two different approaches: the IBM result (grey bar) and the optimal control with (blue bar) and without (green bar) inclusion of hardware noise compared to the exact ground-state distribution (red bar).